Broadband Electromagnetic Modeling of Woven Fabric Composites

Mark S. Mirotznik, *Senior Member, IEEE*, Shridhar Yarlagadda, Raymond McCauley, and Peter Pa, *Student Member, IEEE*

***Abstract*—We demonstrate a new method for predicting the broadband electromagnetic (EM) wave propagation characteristics of woven fabric composites. The method combines a rigorous EM model with effective media theory to predict the EM properties of structural composites from dc to 50 GHz. Experimental results are provided that demonstrate the validity of the method. We also describe the presence of large narrow band electromagnetic resonances that occur above 30 GHz. These resonances, which are shown to be guided mode resonances, can be predicted by solving a simple dispersion relation.**

***Index Terms*—Composites, dielectric properties, effective medium, guided mode resonances, millimeter wave, rigorous couple wave, woven fabrics.**

I. Introduction

WOVEN FABRIC composites are a popular core building block material of many commercial and military platforms in addition to being a common substrate for circuit-board manufacturing. The composite's high strength-to-weight ratio, low cost, and good thermal properties are among some reasons for their popularity. Conventional composites are composed of layers of woven fabrics, usually consisting of glass, polymer, or carbon fibers that are held together by a polymer matrix or resin. Decades of military, academic, and industrial research have gone into the design and manufacturing of composites whose mechanical properties are optimized. Much more recently, material researchers have begun to investigate ways to create composites that have other attractive material properties beyond their mechanical strength, such as electromagnetic (EM) properties [1]–[3]. By tailoring the EM properties of structural composites (e.g., complex permittivity and permeability), it may be possible to integrate antennas, frequency-selective surfaces, and other electromagnetic components directly into the structural skin of future commercial and military vehicles and structures. Such applications would be greatly aided by good predictive models that could be used to select the proper base materials (i.e., fabric type, fabric architecture, and resin) and layered configuration to create a structural composite with attractive EM and mechanical properties. The literature reports several approaches for simulating the EM properties of woven composites. The first uses effective media theory [4]–[6] to provide closed-form approximations for the composite's effective dielectric constant as a function of the dielectric properties of the fiber and resin components and the geometrical architecture of the fabric. Although attractive from a computational perspective, effective media theory is accurate only for fabric architectures in which the length scales (i.e., fabric's unit cell size) are much smaller than the wavelength of illumination. As the wavelength approaches the periodicity of the fabric, which is referred to as the resonance regime, the assumptions on which these closed-form expressions are based are no longer valid. For most structural fabrics, this occurs well within the microwave region, and, for composite substrates used in circuit boards, the resonance regime shifts to even higher frequencies due to weaves with smaller unit cells.

A second approach described by Chin and Lee [7], [8] predicts the dielectric properties of unidirectional composite fabrics and laminates by constructing equivalent lump circuit representations. The circuit models, consisting of parallel *RC* circuits, were shown to accurately predict the effective dielectric properties of composite laminates within the X-band (8–12 GHz). The method was extended to full 3-D woven fabrics by Yao [9]. The circuit analog method becomes less accurate as the frequency increases to the point in which the wavelength approaches the unit cell size.

A third approach utilizes rigorous EM models. Although computationally more difficult, this approach can generate accurate results for woven composites of any fabric architecture [22]. Several different rigorous EM methods can be used for this purpose, including the finite-element method (FEM) and finite-difference time-domain (FDTD) and modal-based solution methods, such as the rigorous coupled wave (RCW) algorithm. The major disadvantage of employing rigorous methods is the computational expense. An FEM model that incorporates the exact geometry of the unit cell, including the fiber bundle, requires hours of computation time on a medium sized workstation.

In this paper, we present a hybrid EM model that combines effective media theory with a rigorous EM method (i.e., RCW method). The end result is a computationally efficient model that predicts the EM properties of woven fabric composites, including resonance effects, at frequencies as high as 50 GHz. Moreover, this method can be easily applied to complicated 2-D and 3-D weave architectures and to multilayered laminates. In

Manuscript received April 05, 2011; revised September 20, 2011; accepted September 29, 2011. Date of publication November 18, 2011; date of current version December 30, 2011. This work was supported by the Office of Naval Research.

The authors are with The University of Delaware, Newark, DE 19716 USA (e-mail: mirotzni@ ece.udel.edu; yarlagad@udel.edu; rei@udel.edu; ppa@udel.edu)

Color versions of one or more of the figures in this paper are available online at http://ieeexplore.ieee.org.

Digital Object Identifier 10.1109/TMTT.2011.2171980

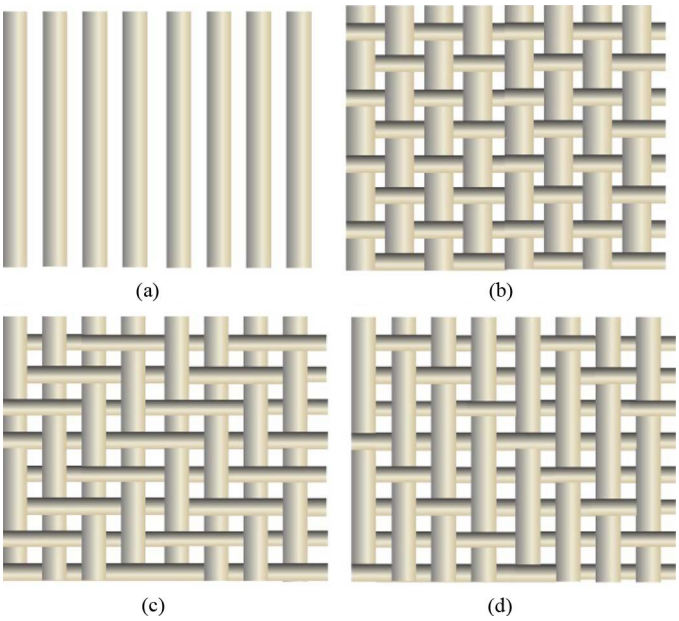

Fig. 1. Common weave architectures used in woven fabric structural composites. (a) 1-D unidirectional weave. (b) 2-D plain weave. (c) 2/2 twill weave. (d) Four harness satin weave.

this paper, experimental validation from 4 to 50 GHz is provided for single layers of dry structural-grade woven glass fabrics and for the same fabrics infused with a vinyl ester resin.

II. Woven Fabric Architectures

Fiber-reinforced plastic (FRP) structures use a large variety of structural-grade woven fabrics. These fabrics vary in fiber type (e.g., glass, carbon, kevlar, or aramid), thickness, weight, and geometrical architecture of the weave. For most applications, a number of fabric layers are stacked in specific orientations and infused with a polymer resin (e.g., thermosets such as epoxy, vinyl ester, or polyester) to create an FRP structure that satisfies the mechanical requirements of the application. In creating electromagnetically functionalized composite structures, choice of the proper fabrics and resins must also take into account the electromagnetic requirements (e.g., low loss and low scattering). The broadband EM properties are sensitive to the choice in fiber type, weave, bundle size, and bulk dielectric properties of the resin.

Here, we present a model that can be used to predict the broadband EM properties of FRPs. For the sake of brevity, we provide illustrative examples for the most common weave architectures (Fig. 1). These are unidirectional and common 2-D weaves. A unidirectional fabric, shown in Fig. 1(a), is composed of a periodic arrangement of fiber bundles aligned along the same axis. It should be noted that each fiber bundle, shown in the figure, is actually composed of thousands of small cylindrical fibers. The cross-sectional shapes of the bundles typically form elongated ellipses with an eccentricity close to unity.

In 2-D weaves, the fiber bundles are aligned along two orthogonal axes. The most common 2-D weaves are the plain, twill, and satin weaves (Fig. 1(b)–(d), respectively). There are a number of other 2-D and 3-D weave types that can also be modeled using the methods described in this paper. Here, we concentrate on modeling only single-layer fabrics—both dry and infused with a polymer resin. However, the described methods can easily be applied directly to the analysis of multilayered composite laminates. For the sake of brevity, we will present the multilayered results in a subsequent manuscript.

III. Approximate EM Representation

Here, we describe the approximate EM representations of the woven fabric composites. Before proceeding, we outline the following objectives of the model: 1) to create an EM model that accurately predicts the EM response of a woven fabric composite over a broad range of frequencies (dc to 50 GHz) where effective media theory becomes invalid; 2) to create an EM model that can be applied directly to a wide variety of fabric and resin types and weave architectures; and 3) to create a model that is computationally efficient and can be integrated subsequently into an iterative design algorithm.

Our approach was to combine effective media theory, where valid, with an efficient rigorous EM algorithm. To this end, we employed the following assumptions to model a single woven fabric layer.

1) The fabric weave has adequate uniformity so that it can be modeled as an infinitely periodic structure.
2) The dielectric properties of the individual fiber bundles shown in Fig. 1(a)–(d) can be approximated by their effective bulk anisotropic properties. This is a reasonable approximation for the frequencies of interest here (i.e., $<$ 50 GHz) since the diameter and spacing of the individual fibers is very small compared with the wavelength. The specific effective media model used for the fiber bundles is discussed in more detail later in this paper.
3) For regions in which two fiber bundles overlap, such as the 2-D weaves shown in Fig. 1(b)–(d), the EM properties are insensitive to the order (i.e., insensitive to which bundle is on the top). Moreover, the dielectric properties within the overlap region are assumed to be an average of the x- and y-directed fiber bundle properties. This is a reasonable approximation as long as the thickness of the fiber bundle is small compared with the wavelength. For most structural-grade fabrics, the bundle thickness is less than $<$ 0.5 mm. Consequently, this approximation will begin to break down as the frequency increases much beyond 50 GHz.
4) The cross-sectional shape of the fiber bundle, which is typically an elongated ellipse, can be approximated as a rectangular cross section of the same cross-sectional area. This is again a reasonable assumption as long as the thickness of the fiber bundle is thin compared with the wavelength.

With these approximations in mind, the EM representations for the unidirectional and 2-D weaves shown in Fig. 1 are now presented.

A. Unidirectional Fabrics

Fig. 2(a) shows a typical unidirectional composite fabric. It also shows the thin polymer stitching thread used to hold the fiber bundles in place. The stitching thread takes up less than

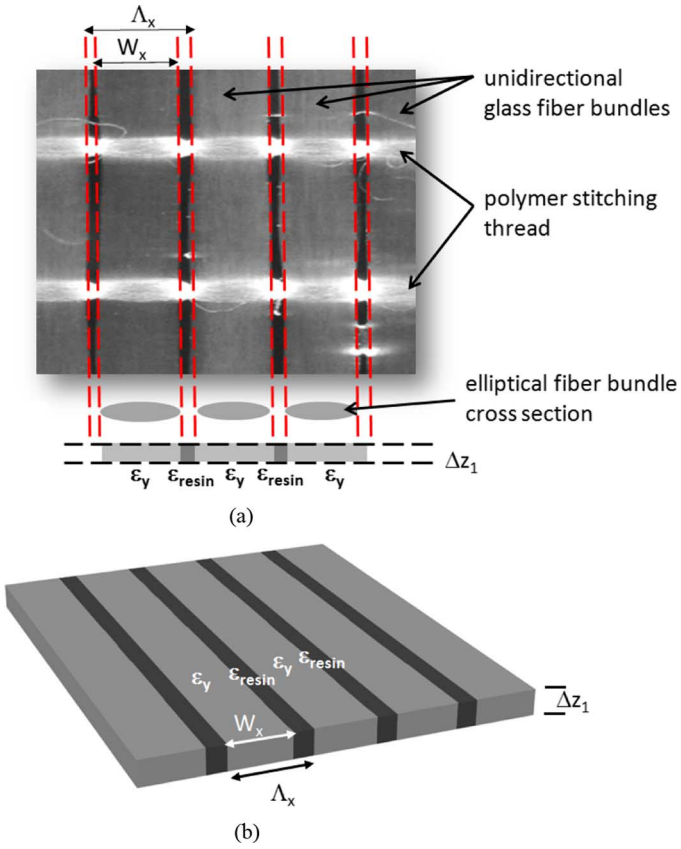

Fig. 2. EM model used to analyze unidirectional composite fabrics.

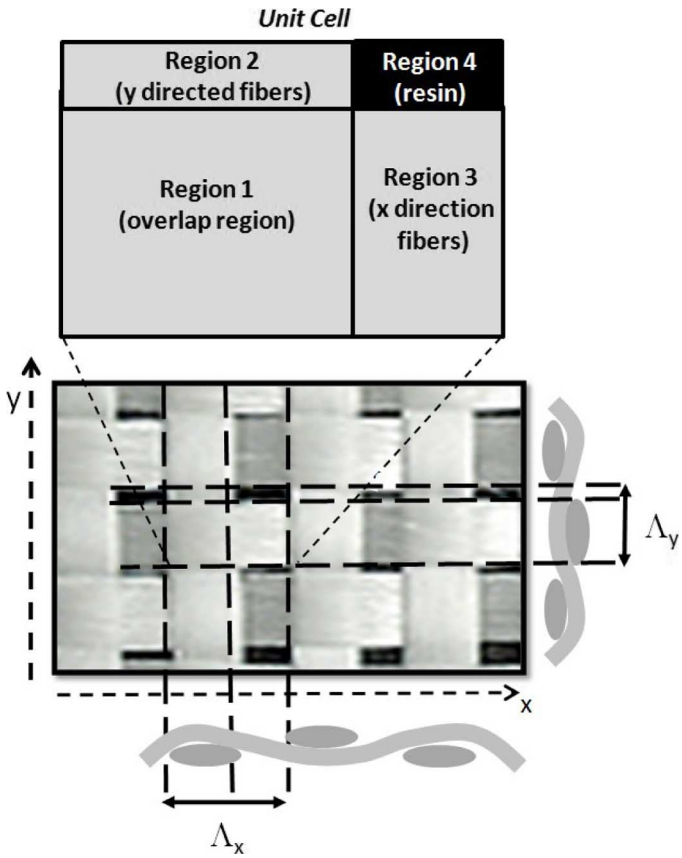

Fig. 3. Planar view of the four-region model used to represent the unit cell of 2-D woven fabrics. The fabric is assumed to be infinitely periodic in both the x- and y-directions with a periodicity of Λ_x and Λ_y, respectively. It should be noted that the periods along the x- and y-axes may not be identical as weaves can be nonsymmetric. This could lead to anisotropic EM properties.

2% of the total fabric volume, and, as a result, its contribution to the fabric's EM properties was considered negligible. Fig. 2(a) illustrates a single layer of a dry fabric in which all spaces not occupied by a fiber, both internal to a fiber bundle and between fiber bundles, are assumed to be free space. However, in the vast majority of applications, this fabric is infused with a resin that fills in all of these unoccupied spaces.

Fig. 2(b) shows the approximate EM representation of the unidirectional fabric. Here, we applied three of the approximations listed previously, namely, that the EM properties of the fiber bundles were modeled as an effective anisotropic material and that the cross-sectional geometry of the fiber bundles was approximated using a rectangular geometry. It is clear that, for the unidirectional fibers, our EM representation is simply a 1-D dielectric grating with anisotropic material properties.

B. 2-D Woven Fabrics—Four-Region Model

Fig. 3 illustrates a standard orthogonal 2-D woven composite fabric with a plain weave. It is constructed with two sets of orthogonal fiber bundles running along the x and y axes. The approximate EM representation of this fabric is presented in Figs. 3 and 4. Applying the four approximations described previously, we construct a unit cell composed of four regions. Region 1 is the portion of the fabric in which the x- and y-directed fiber bundles overlap; regions 2 and 3 contain only the y- and x-directed fiber bundles, respectively; and region 4 is completely unoccupied by fibers. To account for the region where the fiber bundles overlap, the total thickness of the unit cell is twice the thickness of the fiber bundle (i.e., $2\Delta z$). To create a complete fabric this unit cell is periodically replicated with periods of Λ_x and Λ_y along the x and y axes, respectively.

In the z-direction, each unit cell is broken into two equally thick layers [Fig. 4(a)]. The thickness of each layer is assumed to be the thickness (Δz) of a fiber bundle. The bottom layer [Fig. 4(b)] contains the nonoverlapping fiber bundles as well as the overlapping region. The top layer [Fig. 4(c)] only contains the overlapping region. All regions unoccupied by fibers are assumed to be filled with air (fabric model) or resin (composite model). Fig. 4 shows the dielectric properties within each of the various regions. Specifically, $\overline{\overline{\varepsilon}}_1$, $\overline{\overline{\varepsilon}}_2$, and $\overline{\overline{\varepsilon}}_3$, and ε_4 denotes the effective permittivity in each of the four regions illustrated in Figs. 3 and 4. In regions 2 and 3, the permittivity will depend on the orientation of the fiber bundle (e.g., x- or y-directed fibers) and the polarization of the incident field (e.g., x or y linear polarization). This can be described mathematically as permittivity tensors given by

$$\overline{\overline{\varepsilon}}_2 = \begin{bmatrix} \varepsilon_x^{(y)} & 0 \\ 0 & \varepsilon_y^{(y)} \end{bmatrix}$$
$$\overline{\overline{\varepsilon}}_3 = \begin{bmatrix} \varepsilon_x^{(x)} & 0 \\ 0 & \varepsilon_y^{(x)} \end{bmatrix} \quad (1)$$

where the superscripts in (1) refer to the orientation of the fibers and the subscripts denotes the polarization state of the incident

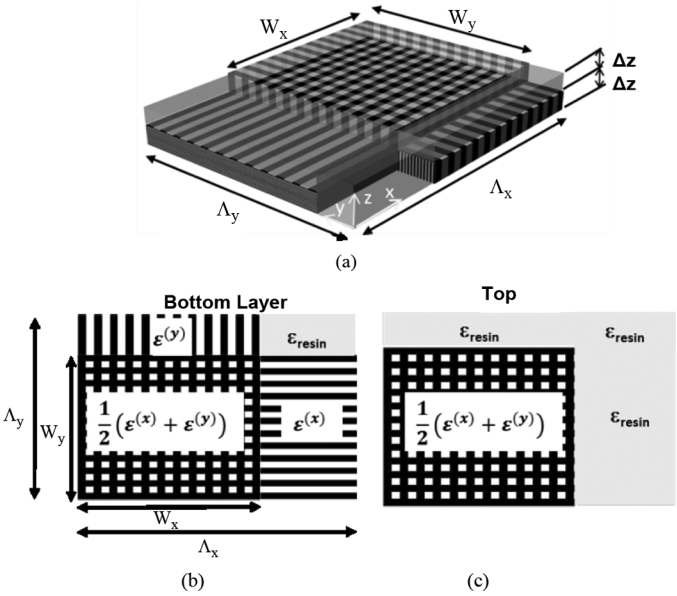

Fig. 4. (a) Detailed 3-D view of the four-region model used to model the fabric's unit cell. In the z-direction, the model is composed of two equally thick layers with dielectric properties shown in (b) and (c).

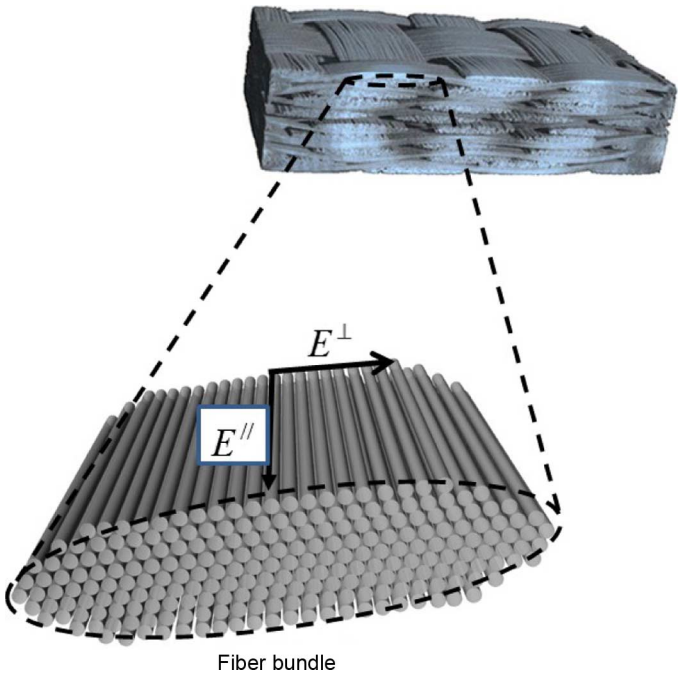

Fig. 5. Illustration of fiber bundles used to create the woven fabrics. Each bundle is comprised of thousands of individual cylindrical fibers.

field. For the case in which the fiber bundles oriented in the x- and y-directions are identical (the most common case), then $\varepsilon_x^{(x)} = \varepsilon_y^{(y)}$ and $\varepsilon_x^{(y)} = \varepsilon_y^{(x)}$. In region 1 of Fig. 3 (i.e., overlapping region) we assume the effective permittivity is simply an average of regions 2 and 3 and is given by

$$\bar{\bar{\varepsilon}}_1 = \frac{1}{2}\left(\bar{\bar{\varepsilon}}_2 + \bar{\bar{\varepsilon}}_3\right). \tag{2}$$

In region 4, the permittivity is scalar equal to the bulk properties of the resin, $\varepsilon_4 = \varepsilon_{\text{resin}}$. The proposed unit cell description is similar to the "mosaic model" used in fabric mechanical property prediction models [10]. In the end, the four-region model of 2-D woven fabrics resembles a double-periodic dielectric-grating structure in which the dielectric properties within the grating are the effective anisotropic properties described above. Once the effective properties are calculated, the EM response of the grating can be determined using a rigorous EM algorithm described in more detail later in this paper.

It should be noted that the EM representation for 2-D woven fabrics remains the same across the standard weave configurations shown in Fig. 1. This results from the fact that the only variation between these weaves is the order, in which the fiber bundles overlap. Since we are assuming that the EM properties are insensitive to that order, the same general model can be employed. Experimental validation for this assumption is provided later in this paper.

C. Effective Dielectric Constant of Individual Fiber Bundles

Each fiber bundle within a composite fabric is itself a heterogeneous mixture of thousands of individual cylindrical fibers packed within a background material or resin (Fig. 5). If we assume that the diameter of each individual fiber is small compared with the wavelength, then we can employ effective media theory to represent the bundle properties as an effective anisotropic bulk medium. Since the diameter of most standard glass or carbon fibers within structural composites is less than 25 μm, this is a reasonable assumption well into the millimeter or even terahertz frequency regimes.

A number of investigators have explored effective media approximations of composite systems that we can apply to our system. In particular, Bal and Kothari [4] reviewed a number of dielectric mixture formulas specific to woven fabrics. Of those formulas, Bruggeman's approximation for 2-D parallel cylinders was the most representative of the fiber bundles encountered in structural composite fabrics. Without any loss in generality, we will assume the fiber bundles to be oriented along the x-axis. Bruggeman's formula calculates the effective anisotropic dielectric properties when the electric field is polarized parallel to the fiber direction as

$$1 - v_f = \frac{\varepsilon_{\text{fiber}} - \varepsilon_{(x)}^{(x)}}{\varepsilon_{\text{fiber}} - \varepsilon_{\text{resin}}} \left(\frac{\varepsilon_{\text{resin}}}{\varepsilon_x^{(x)}}\right)^{1/2} \tag{3}$$

where ν_f denotes the volume fraction of fiber within the bundle, $\varepsilon_{\text{fiber}}$ and $\varepsilon_{\text{resin}}$ denote the bulk permittivity of the fiber and resin components, respectively, and $\varepsilon_x^{(x)}$ represents the effective permittivity for the case of an x-directed fiber bundle with the incident field polarized parallel to the axis of the fibers. If the incident electric field vector is oriented perpendicular to the fiber axis, then the effective media approximation is simply given as a straight volume fraction average

$$\varepsilon_y^{(x)} = v_f \cdot \varepsilon_{\text{fiber}} + (1 - v_f)\varepsilon_{\text{resin}} \tag{4}$$

where $\varepsilon_y^{(x)}$ represents the effective permittivity of the x-directed fiber bundle for the perpendicular polarization case.

The properties for the y-directed fiber bundles of (1) are easily derived from (3) and (4) by a simple substitution of "x for y" and "y for x." It should be noted that the effective dielectric

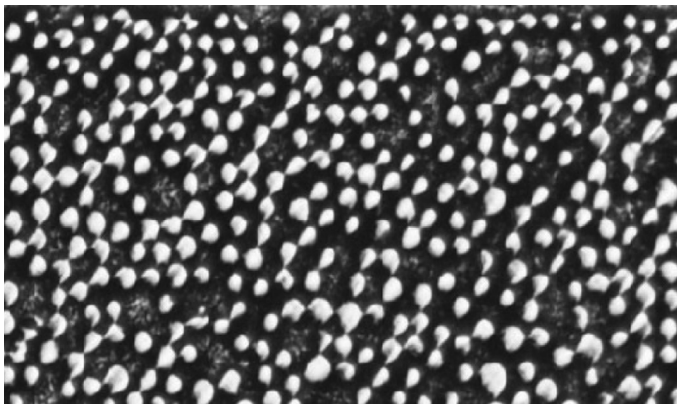

Fig. 6. Micrograph image of the cross section of a typical fiber bundle. The white objects denote the fibers. The image clearly indicates that fiber packing is far from ideal.

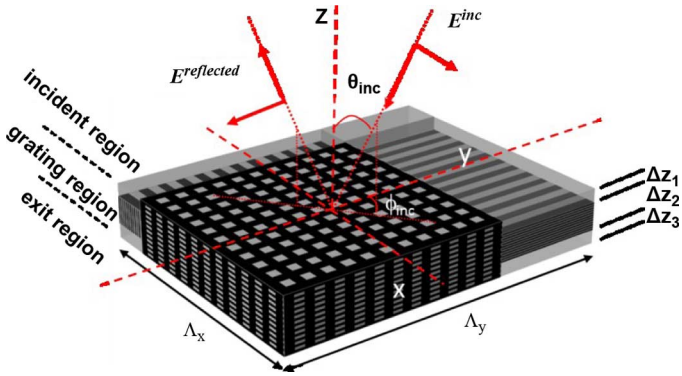

Fig. 7. Solution domain used by the RCW theory to solve for the reflected and transmitted fields from woven fabric composites.

properties of the fiber bundles, calculated using (1)–(4), are reasonably sensitive to the bundle's volume fraction of fiber to resin ν_f. Unfortunately, there is always some uncertainty in determining ν_f. In theory, the maximum theoretical value of ν_f for a tightly hexagonally packed bundle is 92%. However, in reality, the bundles are never perfectly formed, and the volume fraction can be as low at 60%. To arrive at a more accurate estimate, we used cross-sectional microscopy to measure ν_f for a number of fiber bundles. The micrograph image of Fig. 6 illustrates the imperfect arrangement of fibers within a typical bundle. Based on a statistical sampling of various fiber bundle measurements, we arrived at an average volume fraction of fiber to resin of 70%. Thus, throughout the remainder of this paper, we assume $\nu_f = 0.7$ for all numerical simulations.

It should be noted that Bruggeman's formula is applied only for the case of nontwisted fiber bundles. While we believe that the model will still be accurate in the case of fabrics in which the fiber bundles have a slight twist, it would likely need to be revised for the case of highly twisted bundles (e.g., rope-like bundles). Fortunately, the vast majority of structural fabrics do not have twisted bundles.

IV. EM Modeling of Woven Fabric

A. Rigorous Coupled Wave Analysis

To predict the wideband electromagnetic properties of woven fabric composites using the models shown in Figs. 2 and 4, we chose to implement the RCW algorithm originally presented by Moharam and Gaylord [12], [13]. Our specific implementation is based on the enhanced transmittance matrix approach introduced by Moharam *et al.* [14] and later refined by Lalanne [11], [15] and Noponen and Turunen [16].

Using this method, we define regions within the solution domain illustrated in Fig. 7. These are: 1) *an incident region* that is assumed to be an infinite half-space filled with a lossless dielectric of index $n_{\rm inc}$; 2) *an exit region* that is assumed to be another infinite half-space filled with a lossless dielectric of index $n_{\rm exit}$; and 3) *a layered grating region* that contains multiple layers of dielectric slabs with periodic structures. The total thickness of the layered region is

$$Z_{\rm tot} = \sum_{n=1}^{N} \Delta z_n \tag{5}$$

where Δz_n denotes the thickness of each layer and N denotes the total number of layers. The first step in the RCW method is to represent the EM fields in each of the three regions.

1) Incident Region: Within the incident region, denoted as region I, the EM fields consist of an incident plane wave plus all of the diffracted orders reflected from the structure [16]. This is written for the electric fields as

$$\bar{E}_I = \widehat{u} \exp\left(-j\vec{k}_I \cdot \vec{r}\right) + \sum_{m=-\infty}^{\infty} \sum_{n=-\infty}^{\infty} \vec{R}_{mn} \exp\left(-j(\vec{k}_{I,mn} \cdot \vec{r})\right) \tag{6}$$

where $\vec{k}_I$ and $\widehat{u}$ denote the wave vector and unit polarization vector of the incident plane wave, respectively. The second term in (6) accounts for all of the reflected diffractive orders. Since each of the components in (6) represents a plane wave, the magnetic field equations can be easily derived from these. In (6), $\vec{R}_{mn}$ and $\vec{k}_{I,mn}$ denote the vector reflection coefficient and wave vector of the mnth reflected order in region I, respectively. The vector components of $\vec{k}_{I,mn}$, result from the phase-matching and Floquet conditions and are given by

$$\vec{k}_{I,mn} = \hat{u}_x \left[k_o n_{\rm inc} \sin(\theta_{\rm inc}) \cos(\phi_{\rm inc}) - \frac{2\pi m}{\Lambda_x}\right] + \hat{u}_y \left[k_o n_{\rm inc} \sin(\theta_{\rm inc}) \sin(\phi_{\rm inc}) - \frac{2\pi n}{\Lambda_y}\right] - \hat{u}_z k_{Iz,mn} \tag{7}$$

where $\theta_{\rm inc}$ is the polar angle and $\phi_{\rm inc}$ is the azimuth angle of the incident plane wave.

The z-component of the wave vector, given in (7), is written more explicitly as

$$k_{zI,mn} = \begin{cases} \sqrt{(n_{\text{inc}}k_o)^2 - k_{x,m}^2 - k_{y,n}^2}, & k_{x,m}^2 + k_{y,n}^2 < (n_{\text{inc}}k_o)^2 \\ -j\sqrt{k_{x,m}^2 + k_{y,n}^2 - (n_{\text{inc}}k_o)^2}, & k_{x,m}^2 + k_{y,n}^2 > (n_{\text{inc}}k_o)^2 \end{cases} \tag{8}$$

where $k_{x,m}$ and $k_{y,n}$ denote the x and y components of the wave vector given in (7). It is easily deduced from (7) and (8) that, if the grating periods Λ_x and Λ_y are small compared with the incident wavelength $(\lambda_o/n_{\text{inc}})$, only the $(m = n = 0)$ diffractive order will propagate in reflection and transmission (i.e., all other diffractive orders will be evanescent). This condition is written mathematically as

$$\Lambda_x < \frac{\lambda_o}{n_{\text{inc}}\left(1 - \sin(\theta_{\text{inc}})\cos(\phi_{\text{inc}})\right)}$$
$$\Lambda_y < \frac{\lambda_o}{n_{\text{inc}}\left(1 - \sin(\theta_{\text{inc}})\sin(\phi_{\text{inc}})\right)}. \tag{9}$$

2) Exit Region: Within the exit region, denoted as region III, the EM fields consist of all of the diffracted orders transmitted through the structure [16]. This is written for the electric fields as

$$\bar{E}_{III} = \sum_{m=-\infty}^{\infty}\sum_{n=-\infty}^{\infty} \vec{T}_{mn} \exp\left(-j(\vec{k}_{III,mn}\cdot\vec{r})\right). \tag{10}$$

Here, $\vec{T}_{mn}$ and $\vec{K}_{III,mn}$ denote the vector transmission coefficient and wave vector of the mnth transmitted order in region III, respectively. The wave vector in region III takes the same mathematical form as (7) and (8) with the one exception of replacing n_{inc} with n_{exit}. Using a similar analysis to that of region I, it can easily be shown that, to avoid any propagating diffractive orders in the transmitted region other than the $m = n = 0$ term, the grating periods must satisfy the relations

$$\Lambda_x < \frac{\lambda_o}{n_{\text{exit}}\left(1 - \sin(\theta_{\text{inc}})\cos(\phi_{\text{inc}})\right)}$$
$$\Lambda_y < \frac{\lambda_o}{n_{\text{exit}}\left(1 - \sin(\theta_{\text{inc}})\sin(\phi_{\text{inc}})\right)}. \tag{11}$$

3) Multilayered Grating Region: Between the incident and exit regions is a unit cell of the woven fabric composite models illustrated in Figs. 2 and 4.

In the RCW method, the electric and magnetic fields within each layer of the grating region, denoted by the superscript p, are written as a Fourier expansion of spatial harmonics given by

$$\vec{E}_{II}^{p} = \sum_{m=-\infty}^{\infty}\sum_{n=-\infty}^{\infty} \vec{S}_{mn}^{p}(z)\exp(-j(k_{xm}x + k_{yn}y))$$
$$\vec{H}_{II}^{p} = -j\sqrt{\frac{\varepsilon_o}{\mu_o}}\sum_{m=-\infty}^{\infty}\sum_{n=-\infty}^{\infty} \vec{U}_{mn}^{p}(z)\exp(-j(k_{xm}x + k_{yn}y)) \tag{12}$$

where $\vec{U}_{mn}^{p}(z)$ and $\vec{S}_{mn}^{p}(z)$ represent the amplitudes of the spatial harmonics in the pth layer for the magnetic and electric fields, respectively [16]. Substituting (12) into Maxwell's two curl equations and eliminating the z component results in the following coupled system of first-order differential equations for the spatial harmonic amplitudes of (12):

$$\frac{\partial S_{ymn}^{p}(z)}{\partial z} = U_{xmn}^{p}(z) + \frac{k_{yn}}{k_o^2} \times \sum_{q=-\infty}^{\infty}\sum_{r=-\infty}^{\infty} \xi_{m-r,n-q}^{p}(-k_{yq}U_{xrq}^{p} + k_{xr}U_{yrq}^{p})$$
$$\frac{\partial S_{xmn}^{p}(z)}{\partial z} = -U_{ymn}^{p}(z) + \frac{k_{xm}}{k_o^2} \times \sum_{q=-\infty}^{\infty}\sum_{r=-\infty}^{\infty} \xi_{m-r,n-q}^{p}(-k_{yq}U_{xrq}^{p} + k_{xr}U_{yrq}^{p})$$
$$\frac{\partial U_{ymn}^{p}(z)}{\partial z} = \sum_{q=-\infty}^{\infty}\sum_{r=-\infty}^{\infty} \varepsilon_{m-r,n-q}^{p} S_{xrq}^{p} + \frac{k_{ym}}{k_o^2}\left(k_{xm}S_{ymn}^{p} - k_{yn}S_{xmn}^{p}\right)$$
$$\frac{\partial U_{xmn}^{p}(z)}{\partial z} = -\sum_{q=-\infty}^{\infty}\sum_{r=-\infty}^{\infty} \varepsilon_{m-r,n-q}^{p} S_{yrq}^{p} + \frac{k_{xm}}{k_o^2}\left(k_{xm}S_{ymn}^{p} - k_{yn}S_{xmn}^{p}\right) \tag{13}$$

where $\varepsilon_{m,n}^{p}$ and $\xi_{m,n}^{p}$ denote the Fourier components for the permittivity distribution $\varepsilon^{p}(x,y)$, and the inverse permittivity distribution $1/\varepsilon^{p}(x,y)$ of the pth layer given by

$$\varepsilon_{m,n}^{p} = \frac{1}{\Lambda_x\Lambda_y}\int_0^{\Lambda_x}\int_0^{\Lambda_y} \varepsilon^{p}(x,y)\exp\left(-j\left(\frac{2\pi mx}{\Lambda_x} + \frac{2\pi ny}{\Lambda_y}\right)\right)dxdy$$
$$\xi_{m,n}^{p} = \frac{1}{\Lambda_x\Lambda_y}\int_0^{\Lambda_x}\int_0^{\Lambda_y} \frac{1}{\varepsilon^{p}(x,y)}\exp\left(-j\left(\frac{2\pi mx}{\Lambda_x} + \frac{2\pi ny}{\Lambda_y}\right)\right)dxdy. \tag{14}$$

For the geometries of interest here, shown in Figs. 2 and 4, (14) can be solved analytically.

After substituting (14) into (13) and enforcing boundary conditions across all planar interfaces, an eigenvalue problem results that can be solved numerically for the reflected and transmitted diffracted orders $\vec{R}_{mn}$ and $\vec{T}_{mn}$. For a more detailed description of the numerical implementation of RCW, the reader is referred to [12], [15] and [16]. Our custom RCW code, developed using the MATLAB programming environment, was used to calculate the complex transmission and reflection coefficients from woven fabrics.

B. Low-Frequency Effective EM Properties of Woven Structural Fabrics

At frequencies where the wavelength is much larger than the periodicity of the woven fabric ($\lambda_o >> \Lambda_x, \lambda_o >> \Lambda_y$), the EM properties of woven fabrics can be approximated by a bulk anisotropic permittivity derived using simple volume averaging.

For the 1-D unidirectional weaves, illustrated in Fig. 2, the effective permittivity of the fabric is given as

$$\varepsilon_x^{(\text{eff})} = \frac{W_x \varepsilon_x^{(x)} + (\Lambda_x - W_x)\varepsilon_{resin}}{\Lambda_x}$$
$$\varepsilon_y^{(\text{eff})} = \frac{W_x \varepsilon_y^{(x)} + (\Lambda_x - W_x)\varepsilon_{\text{resin}}}{\Lambda_x} \quad (15)$$

where $\varepsilon_x^{(\text{eff})}$ and $\varepsilon_y^{(\text{eff})}$ denote the effective permittivity of 1-D weaves when the incident field is linearly polarized along the x- and y-axes, respectively. Also, in (15), $\varepsilon_x^{(x)}$ and $\varepsilon_y^{(x)}$ denote the effective dielectric properties of the x-directed fiber bundles, described in (1)–(3), and W_x and Λ_x denote the width of the fiber bundles and periodicity of the geometry of the fabric (illustrated in Fig. 2), respectively.

For the 2-D woven fabrics illustrated in Figs. 3 and 4, the effective permittivity of the fabric is given by

$$\varepsilon_x^{\text{eff}} = \varepsilon_{\text{resin}} + \frac{\Lambda_x W_y \left(\varepsilon_x^{(x)} - \varepsilon_{\text{resin}}\right) + \Lambda_y W_x \left(\varepsilon_x^{(y)} - \varepsilon_{\text{resin}}\right)}{2\Lambda_x \Lambda_y}$$
$$\varepsilon_y^{\text{eff}} = \varepsilon_{\text{resin}} + \frac{\Lambda_x W_y \left(\varepsilon_y^{(x)} - \varepsilon_{\text{resin}}\right) + \Lambda_y W_x \left(\varepsilon_y^{(y)} - \varepsilon_{\text{resin}}\right)}{2\Lambda_x \Lambda_y} \quad (16)$$

where $\varepsilon_y^{(\text{eff})}$ and $\varepsilon_y^{(\text{eff})}$ denotes the low-frequency effective permittivity of the 2-D weaves when the incident field is linearly polarized along the x- and y-axes, respectively.

In the following sections, we compare experimental and numerical results for several commonly used structural fabrics using both the RCW method and the effective media expressions given by (15) and (16).

V. Sample Fabrication and Characterization

To experimentally validate the performance of our model, we fabricated a variety of samples and measured the transmissivity and reflectivity from 4 to 50 GHz.

A. Experimental Characterization

To measure the EM response of the samples over a broad frequency range, we employed the free-space focused beam approach illustrated in Fig. 8 and described in numerous publications [17]. To cover the entire 4–50-GHz frequency band, we varied the type and size of the antennas and lenses into four bands. Specifically, within the lower 4–18-GHz band, we used a custom-made focused beam system available at the Naval Surface Warfare Center, Carderock Division. This system integrates custom made large (∼18-in diameter) dielectric lenses to cover the lower frequencies range. Within the K-band (18–26 GHz), Ka-band (26–40 GHz), and U-band (40–50 GHz), we used commercial lens antennas purchased from QuinStar Technology, Inc. Using these systems, we measured the transmittance of each sample using a Agilent PNA vector network analyzer and calibrated using Agilent's standard calibration kits. Time gating was used to remove undesirable reflections from the dielectric lenses and other components within the system. No other postprocessing of the measurement data was conducted.

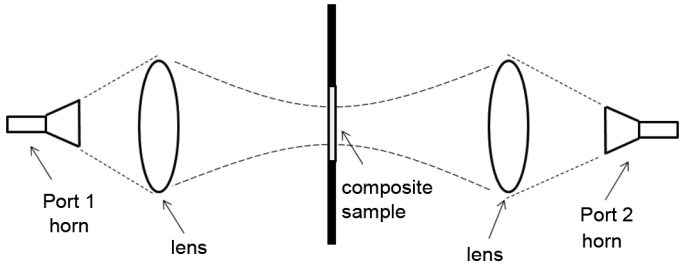

Fig. 8. Free-space focused beam system used to characterize the EM properties of woven fabrics from 4 to 50 GHz.

TABLE I
Composite Samples Used to Validate EM Modeling

	Sample1	Sample2	Sample3	Sample4	Sample5
fiber type	E-glass	E-glass	E-glass	E-glass	E-glass
resin type	no-resin (dry)	510A	no-resin (dry)	510A	no-resin (dry)
weave type	1D	2D plain weave	2D plain weave	2D plain weave	2D plain weave
Fabric weight (oz/yd^2)	16	18	18	24	24
W_x (mm)	1.6	4.4	4.4	4.6	4.6
Λ_x (mm)	1.9	4.5	4.5	5.3	5.3
W_y (mm)	NA	3.9	3.9	4.6	4.6
Λ_y (mm)	NA	6.6	6.6	6.6	6.6
thickness (mm)	0.4	0.7	0.7	0.7	0.7

B. Sample Preparation

To validate the model presented here, over 70 different samples were prepared and tested. The samples varied in fiber and resin type as well as in bundle size and weave architecture. For all of the samples characterized to date, the measured and modeled results show good agreement. For the sake of brevity, detailed results from five of the samples are presented here. Three of the five samples were a single ply of dry woven fabric (i.e., no resin) with different weave architectures. The other two were a single ply of the same woven fabrics infused with an epoxy vinyl ester resin (Derakane 510A) and cured. To create the infused samples, we used the standard vacuum-assisted resin transfer molding (VARTM) process. All samples were mounted in 12-in×12-in frames and characterized using the free-space focused beam system.

Table I lists the relevant material and geometrical information from those samples. Table III presents the effective dielectric properties of the fiber bundles. The listed values are calculated using (2) and (3) and assuming a glass-to-resin volume fraction of 70% and the bulk dielectric properties given in Table II. Here, we assumed the bulk properties of the glass and resin to be frequency-independent. However, since the RCW model is

TABLE II
BULK DIELECTRIC PROPERTIES [WWW.AGY.COM]

	E-Glass	510A Resin
dielectric constant	6.2	3.0
tan(δ)	1.5e-3	1.67e-2

TABLE III
ANISOTROPIC EFFECTIVE MEDIA PROPERTIES OF THE BUNDLES

	Sample1	Sample2	Sample3	Sample4	Sample5
$\varepsilon_y^{(x)}$ and $\varepsilon_y^{(x)}$	3.04	4.93	3.04	4.93	3.04
tan(δ)	6.6e-4	6.9e-3	6.6e-4	6.9e-3	6.6e-4
$\varepsilon_x^{(x)}$ and $\varepsilon_y^{(y)}$	4.64	5.24	4.64	5.24	4.64
tan(δ)	1.5e-3	4.2e-3	1.5e-3	4.2e-3	1.5e-3
$\varepsilon_x^{(eff)}$	5.91	4.66	3.38	4.64	3.29
tan(δ)	6.8e-4	6.9e-3	1.2e-3	6.9e-3	1.2e-3
$\varepsilon_y^{(eff)}$	4.77	4.60	3.08	4.62	3.16
tan(δ)	8.4e-4	7.4e-3	9.7e-4	7.1e-3	1.3e-3

a frequency-domain technique, it can easily handle dispersive materials without modification.

VI. RESULTS

In the following sections, experimental results for the samples described in Table I are compared with predicted results using both the low-frequency effective media theory and our model based on the RCW algorithm. Results are provided for incident fields linearly polarized in the x- and y-directions with respect to the fabric geometry. This is illustrated in Fig. 9.

A. Low-Frequency Effective Media Model Results

Experimental results are first compared with the low-frequency effective media approximations. The transmission coefficient t of the samples, assuming a bulk permittivity calculated using (15) or (16), is given as [19]

$$t = \left(\frac{E_{\text{transmitted}}}{E_{\text{incident}}}\right) = \frac{2\sqrt{\varepsilon_{\text{eff}}}}{2\sqrt{\varepsilon_{\text{eff}}}\cos\left(\frac{4\pi f}{c}\sqrt{\varepsilon_{\text{eff}}}d\right) - j\,(1+\varepsilon_{\text{eff}})\sin\left(\frac{4\pi f}{c}\sqrt{\varepsilon_{\text{eff}}}d\right)} \tag{17}$$

where c is the speed of light in a vacuum, f is the frequency, d is the thickness of the fabric layer, and ε_{eff} is the effective permittivity calculated using either (15) or (16). The transmittance is the squared magnitude of the transmission coefficient given as

$$T = |t|^2 = \left|\frac{E_{\text{transmitted}}}{E_{\text{incident}}}\right|^2. \tag{18}$$

1) Unidirectional Fabrics: Fig. 10 compares the experimental results to the low-frequency effective media predictions, calculated from (17), for the single dry layer of unidirectional fabric that is described as sample #1 in Tables I and II. It is not surprising that both the prediction and the experiment show a distinct anisotropic response. As presented in Table II, the dielectric constant of the fiber bundles has a significant polarization dependence that will be reflected in the transmittance of the fabric. It is interesting, however, that the simple effective media equations do an adequate job of predicting the EM behavior of the unidirectional fabrics over the entire frequency band studied (4–50 GHz). As will be shown later, this is a direct result of the small fiber bundle size (1.6 mm) and the tight spacing between fiber bundles (0.3 mm). While resonant effects are expected to occur, they are likely to be seen beyond the frequency range studied.

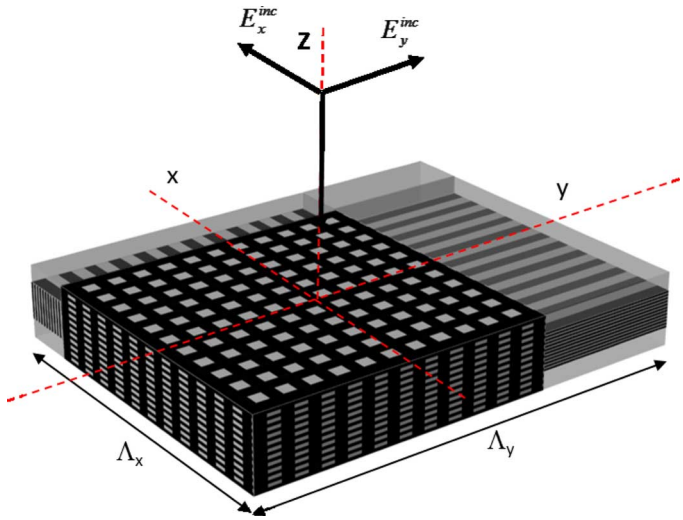

Fig. 9. Coordinate system used to reference the polarization of the incident field with the principal axes of the samples measured.

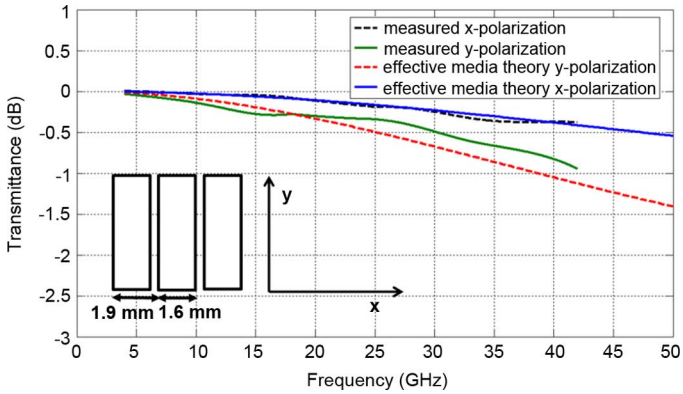

Fig. 10. Effective media theory prediction and experimental results from sample #1 as a function of frequency and polarization. No resin for this sample.

2) 2-D Woven Fabrics: Figs. 11 and 12 compare the experimental results with the low-frequency effective media predictions for the single dry layer of fabrics described as samples #3 and #5 in Tables I and III.

As with unidirectional fabrics, the effective media equations do a reasonable job of predicting the electromagnetic response up to approximately 30 GHz. Unlike the case with 1-D fabrics, however, the anisotropic nature of the response is largely diminished. This is clearly an effect of having two sets of fiber bundles running in orthogonal directions.

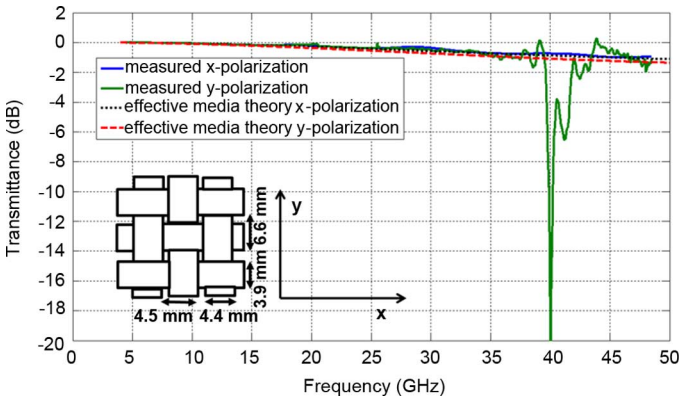

Fig. 11. Effective media theory prediction and experimental results from sample #3 as a function of frequency and polarization. No resin for this sample.

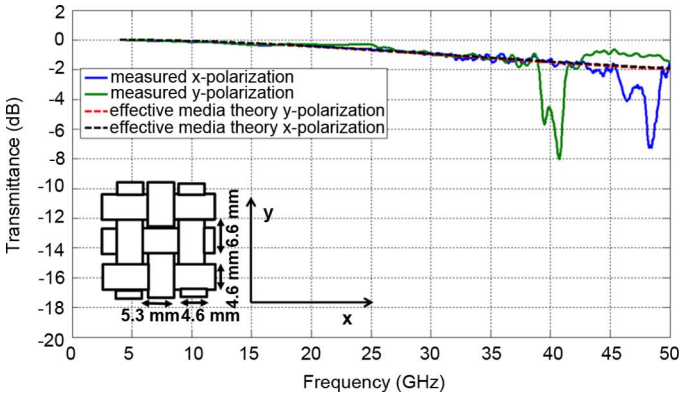

Fig. 12. Effective media theory prediction and experimental results from sample #5 as a function of frequency and polarization. No resin for this sample.

An interesting effect that can be observed in the experimental results for the 2-D fabrics is occurrence of large resonances beyond 30 GHz. These resonances, which are polarization-sensitive, can significantly reduce the transmittance $(-20\ \text{dB})$ even for single layers of thin dry fabrics (i.e., fabrics that are much thinner than the wavelength). The polarization sensitivity of the response, shown very clearly in Fig. 12, is due to the asymmetric properties of some of the fabrics. Later in this paper, we will show that these resonances are, in fact, guided-mode resonance (GMRs) effects. GMRs have been studied for some time within the optics community [19], [20], but, to the best of our knowledge, have never before been observed in woven glass fabrics or in structural composites. The exact spectral locations, amplitudes, and polarization properties of these resonances are a function of the fabric's weave architecture, as well as the bulk dielectric properties of the fiber and resin used.

As a result of GMRs, simple effective media theory will not accurately predict the EM response beyond the frequency of the first GMR. For most structural fabrics, this occurs in the K–Ka-band (18–35 GHz). However, for heavier fabrics in which the fiber bundles are larger and spaced further apart, the resonances can begin to occur at the Ku-band or even within the X-band (8–18 GHz).

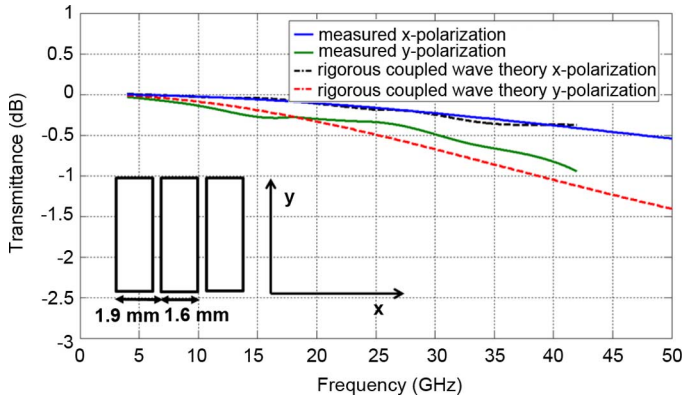

Fig. 13. RCW predicted and experimental results from sample #1 as a function of frequency and polarization. No resin for this sample.

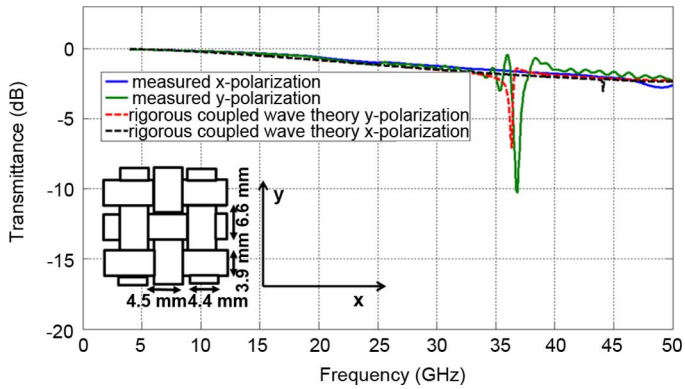

Fig. 14. RCW predicted and experimental results from sample #2 as a function of frequency and polarization. Resin is 510A vinyl ester for this sample.

B. RCW Results

1) Normal Incidence Results: Figs. 13–17 compare the predicted transmittance curves using the new hybrid EM model with the experimental results for samples #1–5. The transmittance was measured using the two orthogonal polarizations described in Fig. 9 at normal incidence.

Fig. 13–17 show that our model adequately predicts the EM responses of all fabrics tested. This includes predicting the polarization-dependent resonant effects seen at the higher frequencies. Comparing Figs. 14–17 also demonstrates how adding polymer resin to the fabric layers shifts the GMRs to lower frequencies and decreases their amplitudes without eliminating them completely. It should be noted the RCW calculations, shown in Figs. 13–17, were computed in less than 30 s using a standard desktop computer. This is well over an order of magnitude faster than the same analysis using the FEM. In Section VII, we will provide a brief analysis of the resonant effects as well as some simple expressions to predict when they are likely to occur.

It should be noted that the measured results in Figs. 16 and 17 reveal two closely spaced resonances for each of the two polarization states. This double resonance effect is not predicted by the model. We believe that this effect is due to the fabric weaves not being perfectly periodic, as was assumed by the RCW model. A slight spatial variation in periodicity produces

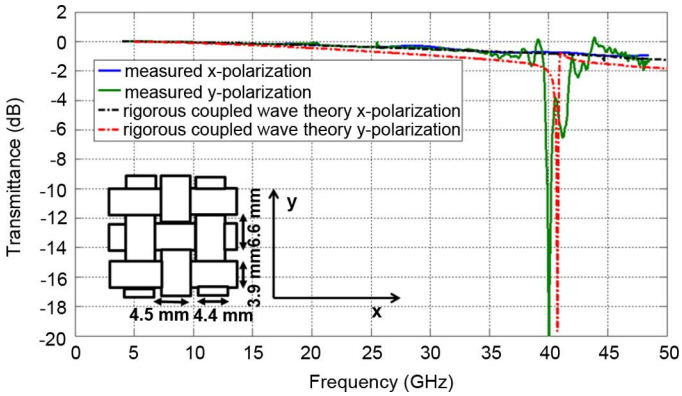

Fig. 15. RCW predicted and experimental results from sample #3 as a function of frequency and polarization. No resin for this sample.

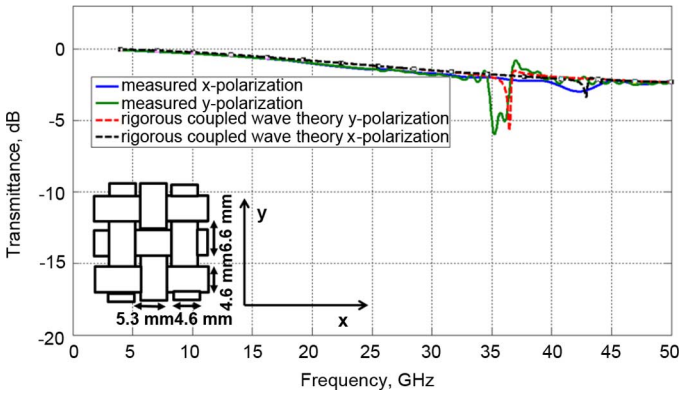

Fig. 16. RCW predicted and experimental results from sample #4 as a function of frequency and polarization. Resin is 510A vinyl ester for this sample.

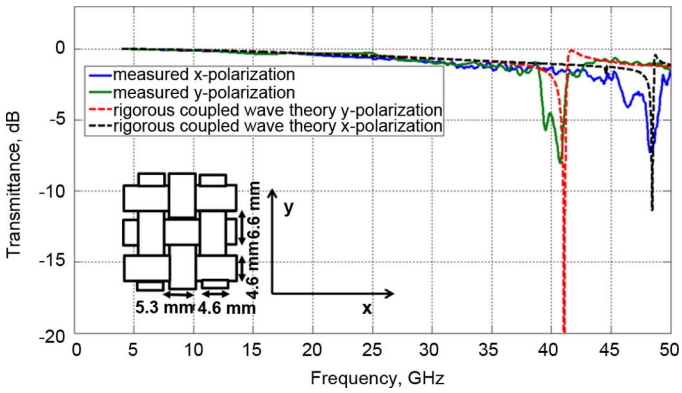

Fig. 17. RCW predicted and experimental results from sample #5 as a function of frequency and polarization. No resin for this sample.

multiple closely spaced resonances in the measured results. Further investigation of this effect is needed to fully understand the discrepancy.

2) Variation With Incidence Angle: Fig. 18 compares the calculated transmittance of sample #2 given in Table I as a function of incidence angle with the measured results. The elevation angle θ_{inc} was varied from 0° to 20°. As predicted by our model and confirmed by measurements, the resonances shift towards lower frequencies as the incidence angle is increased. In

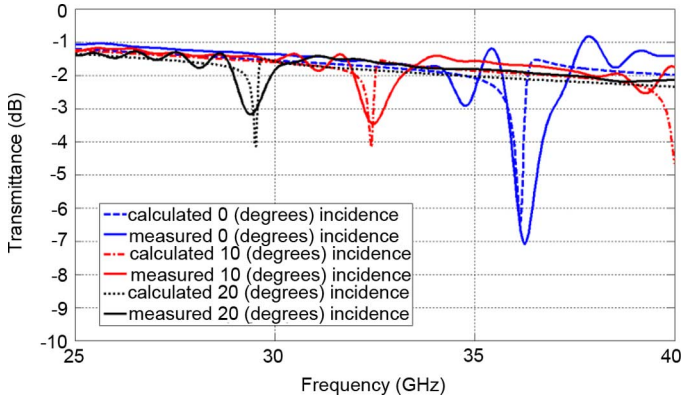

Fig. 18. RCW predicted and experimental results from sample #2 as a function of frequency for several angles of incidence. Resin is 510A vinyl ester for this sample.

Section VII, we will describe the physical nature of these observed resonances.

VII. EM Resonances in Woven Fabrics

It has been shown that, within the microwave regime, common woven fabrics exhibit distinct EM resonances. These effects depend on the architecture of the weave as well as the bulk dielectric properties of the fiber bundles and resin. They have two likely causes: 1) Bragg resonances and 2) GMRs. Bragg resonances occur in periodic structures when higher diffractive orders transition from evanescent to propagating modes. Since woven fabrics to a first order appear electromagnetically as 1-D or 2-D dielectric gratings, it is certainly possible that they could excite Bragg resonances.

It is straightforward to determine the minimum frequency at which the Bragg effects would occur, since it is a simple function of the fabric's periodicity (i.e., Λ_x and Λ_y) and the incident angle illumination θ_{inc}. Specifically, the minimum Bragg frequency is given as [21]

$$f_{\min}^{Bragg} = \frac{300}{(\max(\Lambda_x, \Lambda_x)(1+\sin(\theta_{\text{inc}})))} \text{ GHz.} \qquad (19)$$

For all fabrics studied in this paper (see Table I), we calculated the minimum Bragg frequency to always be greater than 45 GHz at normal incidence. However, our results demonstrate resonances well below 45 GHz. Moreover, our measured resonant frequencies vary significantly as the resin type is changed from air (i.e., no resin) to a polymer resin. Thus, the resonances we are observing are clearly not Bragg effects.

The second likely cause of the resonances is leaky GMRs [19]. A GMR is a phenomenon in which leaky dielectric waveguide modes are excited in the transverse plane of the fabric and then simultaneously re-emitted (illustrated in Fig. 19). At specific resonant frequencies, GMRs can produce very strong reflections in the specular direction.

To a first order, the guided-mode resonant frequencies can be modeled by phase matching the Floquet modes of the dielectric grating (e.g., the fabric) with the transverse dielectric waveguide modes [20]. The waveguide modes are calculated assuming a bulk effective permittivity of the fabric in the transverse plane.

$$\beta_{pq}^{\text{inc}} = \sqrt{\left(\frac{2\pi f_o}{c}\sin(\theta)\cos(\phi) - p\frac{2\pi}{\Lambda_x}\right)^2 + \left(\frac{2\pi f_o}{c}\sin(\theta)\sin(\phi) - p\frac{2\pi}{\Lambda_y}\right)^2} \tag{20e}$$

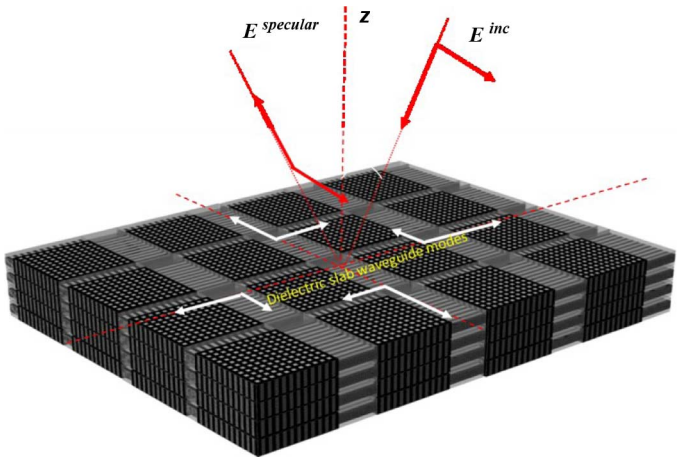

Fig. 19. Illustration of GMRs within a woven fabric composite. Transverse dielectric waveguide modes are excited within the fabric layer or layers in the case of a laminate and then re-emitted, thus producing a strong specular reflection.

TABLE IV
DOMINANT RESONANT FREQUENCIES FOR BOTH x- AND y-POLARIZATION PREDICTED USING THE RCW APPROACH, THE GMR APPROACH, (20) AND COMPARED WITH MEASURED RESULTS[1]

Resonant Frequencies (GHz) Sample Numbers from Tables 1 and 3						
	Sample #	1	2	3	4	5
Predicted (RCW) in GHz	x-polarization	127.3	NA	53.8	42.8	48.4
	y-polarization	132.3	36.2	41.0	36.5	41.0
Predicted GMR Theory in GHz	x-polarization	127.6	47.0	54.5	41.6	48.2
	y-polarization	133.4	36.1	40.1	35.2	40.1
Measured in GHz	x-polarization	NA	NA	NA	42.3	48.4
	y-polarization	NA	36.8	39.9	35.5	41.0

For the 2-D woven fabrics, this results in the set of equations given in

$$\tan(k_{pq}d) = \frac{2k_{pq}\gamma_{pq}}{k_{pq}^2 - \gamma_{pq}^2}TM \tag{20a}$$

$$\tan(k_{pq}d) = \frac{2\varepsilon_{\text{eff}}k_{pq}\gamma_{pq}}{k_{pq}^2 - \varepsilon_{\text{eff}}^2\gamma_{pq}^2}TE \tag{20b}$$

$$k_{pq} = \sqrt{\varepsilon_{\text{eff}}\left(\frac{2\pi f_o}{c}\right)^2 - \beta_{pq}^{inc^2}} \tag{20c}$$

$$\gamma_{pq} = \sqrt{\beta_{pq}^{inc^2}\left(\frac{2\pi f_o}{c}\right)^2} \tag{20d}$$

and β_{pq}^{inc}, shown at the top of this page. These can be numerically solved for the resonant frequencies of the TE and TM dielectric waveguide modes. In (20), d is the thickness of the fabric layer, ε_{eff} denotes the effective permittivity calculated using (15) or (16), c is the speed of light in a vacuum, ϕ and θ are the incident angles shown in Fig. 7, and f_o denotes the resonant frequency. For a given sample and incident field, the equations given in (20) can be solved numerically for all of the allowable GMR frequencies. The dominant (or lowest frequency) modes for our fabrics were the TE_{01} and TE_{10} modes for the x-and y-polarized incident field, respectively. Table IV compares the dominant guided-mode resonant frequencies that were calculated using (20) with the measured resonant frequencies for samples #2–#5.

As illustrated in Table IV, the approximate GMR approach was able to predict the dominant resonance frequencies of woven fabric composites within 10% of the RCW predictions and the measured results.

VIII. DISCUSSION AND CONCLUSION

We have presented a hybrid EM model that combined effective media theory with the RCW method to model the EM properties of woven fabric composites. The method was shown to accurately predict measured results including resonant effects not predicted using pure effective media theory. We also demonstrated for the first time, ti the best of our knowledge, GMRs that occur in standard structural-grade woven composite fabrics and laminates. These resonances, which occur at subwavelength frequency, can be approximately modeled using simple dielectric waveguide theory.

In future work, we will extend the methods and results given here to multilayered composite laminates. We will also present results for more complicated 2-D and 3-D woven fabrics as well as custom-designed composite fabrics with heterogenous combinations of fiber types. By doing so, we will show that it is not only possible to predict the EM behavior of structural composites, but also to actually tailor it for particular applications.

REFERENCES

[1] S. C. Nemat-Nasser, A. Amirkhizi, T. Plaisted, J. Isaacs, and S. Nemat-Nasser, "Structural composites with integrated electromagnetic functionality," in *Proc. SPIE*, 2002, vol. 4698, pp. 237–245.
[2] T. Plaisted, A. Amirkhizi, D. Arbelaez, S. C. Nemat-Nasser, and S. Nemat-Nasser, "Self-healing structural composites with electromagnetic functionality," in *Proc. SPIE*, 2003, vol. 5054.
[3] M. S. Mirotznik, B. Good, P. Ransom, D. Wikner, and J. N. Mait, "Design of inverse moth-eye antireflective surfaces," *IEEE Trans. Antennas Propag.*, vol. 58, no. 9, pp. 2969–2980, Sep. 2010.
[4] K. Bal and V. K. Kothari, "Permittivity of woven fabrics: A comparison of dielectric formulas for air-fiber mixture," *IEEE Trans Dielectr. Electr. Insulation*, vol. 17, no. 3, pp. 881–889, Jun. 2010.
[5] R. Agarwal and A. Dasgupta, "Prediction of electrical properties of plain-weave fabric composites for printed wiring board design," *J. Electron. Packaging*, vol. 115, no. 2, pp. 219–224, Jun. 1993.
[6] S. Rikte, M. Andersson, and G. Kristensson, "Homogenization of woven materials," *Int. J. Electron. Commun.*, vol. 53, no. 5, pp. 261–271, 1999.

[1]Note: NA in the above when either the resonant frequency is beyond our measurement range (4–50 GHz) or if a particular resonance was not detectable.

[7] W. Chin and D. Lee, "Binary mixture rule for predicting the dielectric properties of unidirectional E-glass/epoxy composite," *Composite Structures*, vol. 74, pp. 153–162, 2006.
[8] W. Chin and D. Lee, "Laminating rule for predicting the dielectric properties of E-glass/epoxy laminate composite," *Composite Structures*, vol. 77, pp. 373–382, 2007.
[9] L. Yao, X. Wang, F. Liang, R. Wu, B. Hu, Y. Feng, and Y. Qiu, "Modeling and experimental verification of dielectric constants for three-dimensional woven composites," *Composites Sci. Technol.*, vol. 68, pp. 1794–1799, 2008.
[10] J. Byun and T. Chou, "Modeling and characterization of textile structural composites: A review," *J. Strain Anal. Eng. Design*, vol. 24, no. 4, pp. 253–262, 1989.
[11] P. Lalanne and J. Hugonin, "High-order effective-medium theory of subwavelength gratings in classical mounting: Application to volume holograms," *J. Opt. Soc. Amer. A*, vol. 15, pp. 1843–1851, 1998.
[12] M. G. Moharam and T. K. Gaylord, "Rigorous coupled-wave analysis of planar-grating diffraction," *J. Opt. Soc. Amer. A*, vol. 71, pp. 811–818, 1981.
[13] M. G. Moharam, E. B. Grann, D. A. Pommet, and T. K. Gaylord, "Formulation for stable and efficient implementation of the rigorous coupled wave analysis of binary gratings," *J. Opt. Soc. Amer. A*, vol. 12, pp. 1068–1076, 1995.
[14] M. G. Moharam, D. A. Pommet, and E. B. Grann, "Stable implementation of the rigorous coupled-wave analysis for surface relief gratings: Enhanced transmittance matrix approach," *J. Opt. Soc. Amer. A*, vol. 12, pp. 1077–1086, 1995.
[15] P. Lalanne, "Improved formulation of the coupled-wave method for two-dimensional gratings," *J. Opt. Soc. Amer. A*, vol. 14, pp. 1592–1598, 1997.
[16] E. Noponen and J. Turunen, "Eigenmode method for electromagnetic synthesis of diffractive element with three-dimensional profiles," *J. Opt. Soc. Amer. A*, vol. 11, pp. 2494–2502, 1994.
[17] J. Musil and F. Zacek, *Microwave Measurements of Complex Permittivityby Free-Space Methods and Their Applications*. New York: Elsevier, 1986.
[18] C. Balanis, *Advanced Engineering Electromagnetics*. New York: Wiley, 1989.
[19] S. Wang and R. Magnusson, "Theory and applications of guide-mode resonance filters," *Appl. Opt.*, vol. 13, no. 14, pp. 2606–2613, May 1993.
[20] S. Wang, R. Magnusson, and J. Bagby, "Guided-mode resonances in planar dielectric-layer diffraction gratings," *J. Opt. Soc. Amer. A*, vol. 7, no. 8, pp. 1470–1474, Aug. 1990.
[21] B. Munk, *Frequency Selective Surfaces: Theory and Design*. New York: Wiley, 2000.
[22] V. Volski and G. Vanderbosch, "Full-wave electromagnetic modeling of fabrics and composites," *Composites Sci. Technol.*, vol. 69, pp. 161–168, 2009.

Mark S. Mirotznik (S'87–M'92) received the B.S.E.E. degree from Bradley University, Peoria, IL, in 1988, and the M.S.E.E. and Ph.D. degrees from the University of Pennsylvania, Philadelphia, in 1991 and 1992, respectively.

From 1992 to 2009, he was a Faculty Member with the Department of Electrical Engineering, The Catholic University of America, Washington, DC. Since 2009, he has been an Associate Professor and Director of Educational Outreach with the Department of Electrical and Computer Engineering, University of Delaware, Newark. In addition to his academic positions, he an associate editor of the *Journal of Optical Engineering* and is a Senior Research Engineer for the Naval Surface Warfare Center (NSWC), Carderock Division. His research interests include applied electromagnetics and photonics, computational electromagnetics and multifunctional engineered materials.

Prof. Mirotznik was the recipient of the 2010 Wheeler Prize Award for Best Application Paper in the IEEE TRANSACTIONS ON ANTENNAS AND PROPAGATION.

Shridhar Yarlagadda received the B.Tech. degree from Indian Institute of Technology, Madras, India, in 1989, and the M.S. and Ph.D. degrees from The Pennsylvania State University, University Park, in 1992 and 1999, respectively, all in aerospace engineering.

Since 1997, he has been with the Center for Composite Materials, University of Delaware, Newark. He is currently the Assistant Director for Research with the Center and holds an Adjunct Faculty appointment with the Department of Electrical and Computer Engineering, University of Delaware. His research interests include multifunctional composite materials, novel composite processing methods, and hybrid composite materials for improved durability and damage tolerance.

Raymond A. McCauley received the B.M.E. degree from the University of Delaware, Newark, in 2009, where he is currently working toward the M.S. degree in mechanical engineering.

He has participated in undergraduate research with micro robotics and completed a summer internship with NASA Langley under the DEVELOP program in 2008. Since 2008, he has been a member of SAMPE and plays a key role in the annual composite bridge and wing competition at the University of Delaware.

Peter Pa (S'11) received the B.S. degree in electrical engineering from the University of Delaware, Newark, in 2011, where he is currently working toward the Ph.D. degree in electrical and computer engineering.

His research interests are computational electromagnetics, electromagnetic properties of materials, and engineered electromagnetic materials.